Gibbs phenomenon and the emergence of the steady-state in quantum transport

Michael Zwolak[1, a)]

Biophysics Group, Microsystems and Nanotechnology Division, Physical Measurement Laboratory,
National Institute of Standards and Technology, Gaithersburg, MD 20899, USA

Simulations are increasingly employing explicit reservoirs – internal, finite regions – to drive electronic or particle transport. This naturally occurs in simulations of transport via ultracold atomic gases. Whether the simulation is numerical or physical, these approaches rely on the rapid development of the steady state. We demonstrate that steady state formation is a manifestation of the Gibbs phenomenon well-known in signal processing and in truncated discrete Fourier expansions. Each particle separately develops into an *individual* steady state due to the spreading of its wave packet in energy. The rise to the steady state for an individual particle depends on the particle energy – and thus can be slow – and ringing oscillations appear due to filtering of the response through the electronic bandwidth. However, the rise to the total steady state – the one from all particles – is rapid, with timescale π/W, where W is the bandwidth. Ringing oscillations are now also filtered through the bias window, and they decay with a higher power. The Gibbs constant – the overshoot of the first ring – can appear in the simulation error. These results shed light on the formation of the steady state and support the practical use of explicit reservoirs to simulate transport at the nanoscale or using ultracold atomic lattices.

An increasing number of nanoscale electronic[1–6] studies aim at probing and exploiting dynamical phenomena at both slow and fast timescales[7–17]. Moreover, finite, closed ultra-cold atomic systems[18,19] simulate transient transport[20–28] and can examine the generation of topological matter via time-dependent fields[29,30]. An avenue to computationally study transient and dynamical phenomena is to include particle reservoirs explicitly in the simulation, essentially letting a "capacitor" discharge and drive current through a region of interest[31–49]. The inclusion of relaxation can give a true steady state while still permitting the examination of transient/dynamical processes[50–52] (including for thermal transport[53–55]). This type of "open" system approach has a long history[56,57] (see discussion in Ref. 52), including designs for time-dependent density functional theory (TD-DFT)[58–60]. However, large-scale numerical simulations (e.g., integrating correlation matrices, numerical renormalization and tensor network methods, TD-DFT, or other techniques) generally do not give direct insight into the formation of the steady state and the factors controlling transient behavior.

Here, we employ a Kubo approach to study transients in closed, noninteracting fermionic systems. We demonstrate its application using a system set out of equilibrium by connecting initially disjoint lattices, see Fig. 1, a technique related to the tunneling Hamiltonian and Green's function approaches to transport. We show how the steady state arises, how oscillations decay, and how different frequency scales contribute to transport, as well quantify aspects of simulation error. We expect that this approach will find application in dynamical, many-body transport in both nanoscale and ultracold atomic systems, including diagnosing pathological numerical setups and increasing simulation efficiency.

Before the lattices come into contact (i.e., for times $t < 0$ in Fig. 1), the Hamiltonian is

$$H_0 = H_\mathcal{L} + H_\mathcal{R}, \tag{1}$$
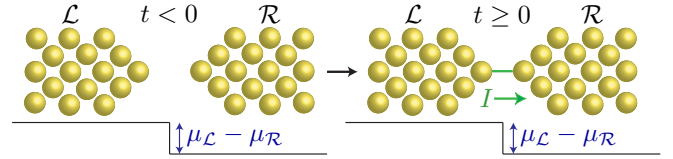
a)Electronic mail: mpz@nist.gov

Figure 1. Schematic of a lattice set out of equilibrium by adding a link at time $t = 0$ between two initially disconnected regions $\mathcal{L}$ and $\mathcal{R}$. There is a density imbalance (black line) that creates a chemical potential drop $\mu_\mathcal{L} - \mu_\mathcal{R}$ (alternatively, there can initially be a uniform potential and a bias simultaneously turns on when connecting the lattice). The current, I, is the step response to the addition of the link (green) filtered by the electronic bandwidth and bias window.

with

$$H_\mathcal{L} = \sum_{k \in \mathcal{L}} \hbar\omega_k a_k^\dagger a_k, \ H_\mathcal{R} = \sum_{k \in \mathcal{R}} \hbar\omega_k b_k^\dagger b_k \tag{2}$$

and $a_k^\dagger$ (a_k) and $b_k^\dagger$ (b_k) are the fermionic creation (annihilation) operators on the left ($\mathcal{L}$) and right ($\mathcal{R}$), respectively. These are noninteracting lattices with $N_{\mathcal{L}(\mathcal{R})}$ levels and frequencies ω_k. The initial state is one with a density imbalance, where the left region has particles up to the chemical potential $\mu_\mathcal{L}$ and the right to $\mu_\mathcal{R}$. This drives the current when, at $t = 0$, the perturbing Hamiltonian

$$H' = \sum_{k \in \mathcal{L}, k' \in \mathcal{R}} \hbar v_{kk'} \left(a_k^\dagger b_{k'} + b_{k'}^\dagger a_k \right) \tag{3}$$

connects the two lattices, as shown in Fig. 1. The strength of the connection is the total hopping frequency $v = \sqrt{\sum_{k,k'} v_{kk'}^2}$, which we will treat as a perturbation. The density imbalance encodes the chemical potential in the initial state, making the calculations non-perturbative in the bias[61] (unlike, e.g., Refs. 62–64, which employ numerical renormalization in tandem with a Kubo approach with the applied bias as the perturbation). We can relate this to a real-

space model with contact at, e.g., one site via the identification $c_1 = \sum_k \mathcal{U}_{1k} a_k$, $d_1 = \sum_k \mathcal{V}_{1k} b_k$ and $v_{kk'} = v\mathcal{U}_{k1}^\star \mathcal{V}_{1k'}$, giving the connection $\hbar v \left(c_1^\dagger d_1 + d_1^\dagger c_1 \right)$. Here, the quantities $\mathcal{U}$ and $\mathcal{V}$ are the transformation matrices from energy- to real-space on the left and right lattices.

We will apply the Kubo formula

$$\langle O\left(t\right)\rangle = \langle O\rangle_0 - \imath \int_0^t dt' \langle [O\left(t\right), H'\left(t'\right)]\rangle_0 \qquad (4)$$

for the observable O, where $O(t) = e^{\imath H_0 t} O e^{-\imath H_0 t}$ is an operator in the interaction picture and $\langle O\rangle_0$ indicates an average with respect to the initial state. While our focus is on closed, finite systems, we will take the infinite system limit to make some expressions more transparent. This will not obscure their interpretation for finite systems.

The particle current from left to right is

$$I(t) = -\langle dN_\mathcal{L}/dt\rangle = -2\sum_{k,k'} v_{kk'} \Im\langle a_k^\dagger b_{k'}(t)\rangle \qquad (5)$$

for $t \geq 0$. Here, $N_\mathcal{L}$ is the number operator in the Heisenberg picture on the left, $dN_\mathcal{L}/dt = -\imath\,[N_\mathcal{L}, H_0 + H']$, and the factor of 2 appears due to taking the imaginary component $\Im$ (i.e., not due to spin). Applying Eq. (4) to $a_k^\dagger b_{k'}(t)$ yields

$$\langle a_k^\dagger b_{k'}(t)\rangle = -v_{kk'}\left(n_k - n_{k'}\right)\frac{e^{\imath t(\omega_k - \omega_{k'})} - 1}{\omega_k - \omega_{k'}}, \qquad (6)$$

where n_k are the initial particle occupancies and we use that $\langle a_k^\dagger b_{k'}\rangle_0 = 0$ for two initially disjoint lattices. The total current from this perturbative result is thus

$$I(t) = 2\sum_{k,k'} v_{kk'}^2 \left(n_k - n_{k'}\right)\frac{\sin\left[(\omega_k - \omega_{k'})t\right]}{\omega_k - \omega_{k'}}. \qquad (7)$$

So far we only assume that the two lattices are initially disconnected and have occupancies from their separate single-particle eigenstates.

Let's first examine the current, $I_k(t)$, from a particle in state k on the left going into an empty reservoir of bandwidth W on the right. Setting $v_{kk'} = v/\sqrt{N_\mathcal{L} N_\mathcal{R}}$ – i.e., a flat band – and taking $\sum_{k'} 1/N_\mathcal{R} \to \int d\omega/W$, gives

$$I_k(t) = \frac{2v^2}{N_\mathcal{L} W}\int_{-W/2}^{W/2} d\omega'\frac{\sin\left[(\omega_k - \omega')t\right]}{\omega_k - \omega'}. \qquad (8)$$

When $t \to \infty$, the integrand approaches $\pi\delta\left(\omega_k - \omega'\right)$, expressing conservation of energy in the absence of inelastic processes and in the long-time limit. This indicates the presence of a steady state current of $2v^2\pi/N_\mathcal{L} W$ even if $N_\mathcal{L} = 1$ (and, since there is only one particle, it can be a fermion or a massive boson). However, the perturbative expression does not capture that there is a decay time[65] $T^\star = N_\mathcal{L} W/2v^2\pi$. For times much shorter than this, the particle looks to be in a steady state. This demonstrates that constructive contributions from many incoming particles are not necessary for steady state formation, but rather it is the spread of a single particle into many different states – its wave-like nature in energy
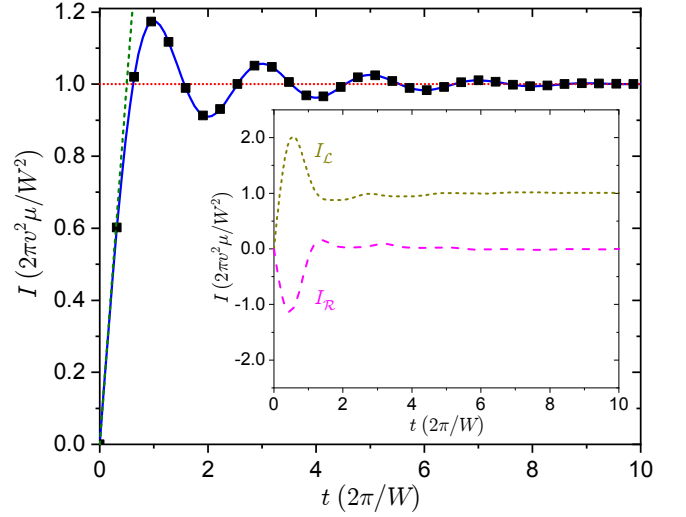

Figure 2. Current through a weak link when density-imbalanced flat band lattices come into contact. The blue line (black squares) shows the Kubo (exact) result for $\upsilon = W \cdot 10^{-3}$, $\mu = W/10$, and $N_{\mathcal{L}(\mathcal{R})} = 100$. The dotted red line is the steady state current and the dashed green line the rise to the steady state at time π/W. Since this is a finite system, the resultant current goes into a "quasi"-steady state. The inset shows the forward, $I_\mathcal{L}$ [$n_k = 1$ and $n_{k'} = 0$ in Eq. (7)], and backward, $I_\mathcal{R}$ [$n_k = 0$ and $n_{k'} = 1$ in Eq. (7)] currents. These have significantly larger transients but they partially cancel, leaving more regular – but algebraically decaying – oscillations in I. A true steady state will form when $N \to \infty$ and then $t \to \infty$.

space – that results in a nearly steady current. Since only a single particle is present, the steady state is just a linear increase in time of the probability for the particle to be in $\mathcal{R}$, which is possible to measure in cold atom lattices by repetition of the experiment many times.

For finite times, the integral in Eq. (8) is just

$$I_k(t) = \frac{2v^2}{N_\mathcal{L} W}\left\{\text{Si}\left[t(\omega_k + W/2)\right] - \text{Si}\left[t(\omega_k - W/2)\right]\right\}, \qquad (9)$$

where $\text{Si}[\circ]$ is the sine integral. The derivative $dI/dt|_{t=0}$ determines the rise to the steady state. For the single particle, this depends on the smaller of the two energies, $|\omega_k + W/2|$ or $|\omega_k - W/2|$. For instance, for $\omega_k = 0$, the initial (linear) rise occurs with slope $2v^2/N_\mathcal{L}$. Thus, the time to reach the steady state value, $2v^2\pi/N_\mathcal{L} W$, is π/W, at which time the current begins oscillating. If ω_k (in $\mathcal{L}$) approaches the band edge (in $\mathcal{R}$), then the steady state takes a long time to develop. In that case, there is a fast process – where one of the sine integral quickly rises – and a slow process – where the other rises with time $\sim 1/(W/2 - |\omega_k|)$. After the initial rise, oscillations – ringing – appear, which decay as the steady state is approached which decay as the steady state is approached. Such oscillations are seen in extended reservoir, microcanonical, and related approaches, in addition to numerical integration of the time-dependent Green's functions[66].

For $\omega_k = 0$, the rapid rise and "ringing oscillation" is none other than Gibbs phenomenon[67–71] for the step function

sign $[t]$ sent through a low-pass frequency filter. The Fourier transform of sign $[t]$ is $\imath\sqrt{2/\pi}/\omega$. Filtering the frequencies outside of the bandwidth $[-W/2, W/2]$ and taking the inverse transform gives Eq. (8) up to a prefactor[72]. The oscillations are thus an inherent aspect of electronic transport. Moreover, the "overshoot" of the current – its first and maximum oscillation overtop the steady state value – is $G \cdot 2v^2\pi/NW$, where $G = 2\mathrm{Si}\,[\pi]/\pi - 1 = 0.1789\ldots$ is the Gibbs constant. That is, the overshoot is about 18 % higher than the steady state value. Regardless of the bandwidth, the magnitude of the overshoot – and, indeed, the dimensionless form of the current – stays the same. When examining $\omega_k \neq 0$, these basic insights remain but now the filter acts asymmetrically, introducing oscillations that depend on both W and ω_k. Different spectral densities of the reservoirs and strong coupling will give different overshoot values. However, the physical process is universal, the signal is filtered through the bandwidth giving rise to ringing oscillations.

We now examine the total current in the presence of a chemical potential drop. Considering the flat band case and equal bandwidths in $\mathcal{L}$ and $\mathcal{R}$, the continuum limit of Eq. (7) gives

$$I(t) = \int_{-W/2}^{W/2} d\omega \, \delta I(\omega, t), \qquad (10)$$

where the contribution to the current at frequency ω in $\mathcal{L}$ is

$$\delta I = \frac{2v^2}{W^2} \int_{-W/2}^{W/2} d\omega' \, [n_\mathcal{L}(\omega) - n_\mathcal{R}(\omega')] \frac{\sin[(\omega - \omega')t]}{\omega - \omega'}. \qquad (11)$$

We now explicitly label the occupancies $n_{\mathcal{L}(\mathcal{R})}$. The steady state current is $2\pi v^2 \mu/W^2$ for a chemical potential drop of $\mu = \mu_\mathcal{L} - \mu_\mathcal{R}$. Equations (10) and (11) show that, to highest order in v, there is a one way flow from filled states on the left into empty states on the right lattice when $\mu_\mathcal{L} > \mu_\mathcal{R}$. Indeed, as with Eq. (8), states at frequency ω go into states $\omega' = \omega$ as $t \to \infty$, giving the standard bias window.

Taking $\mu_\mathcal{L} = \mu/2$, $\mu_\mathcal{R} = -\mu/2$, and performing the integrations at zero temperature (so $n_{\mathcal{L}(\mathcal{R})} = 0$ or 1) yields

$$I(t) = \frac{2v^2}{W^2} \left\{ \sum_{\pm} \pm(W \pm \mu)\mathrm{Si}\left[\frac{t}{2}(W \pm \mu)\right] \right.$$
$$\left. + \frac{4\sin\left[\frac{Wt}{2}\right]\sin\left[\frac{\mu t}{2}\right]}{t} \right\} \qquad (12)$$

$$\approx \frac{4v^2}{W^2}\mathrm{Si}\,[Wt/2]\,\mu, \qquad (13)$$

where the second expression is for a small bias, showing exactly the same manifestation of Gibbs phenomenon as the individual particles at the Fermi level. Figure 2 shows the Kubo result, Eq. (12), together with the exact result for a finite system, as well as the steady state value and initial rise. Just like individual particles at the Fermi level, the total current rises with time π/W. Unlike individual particles, this result is nearly true even when a small frequency scale appears in Eq. (12), e.g., $(W - \mu)$ for a chemical potential drop comparable to the bandwidth. The component with the small frequency scale takes a longer time to reach its steady state but it
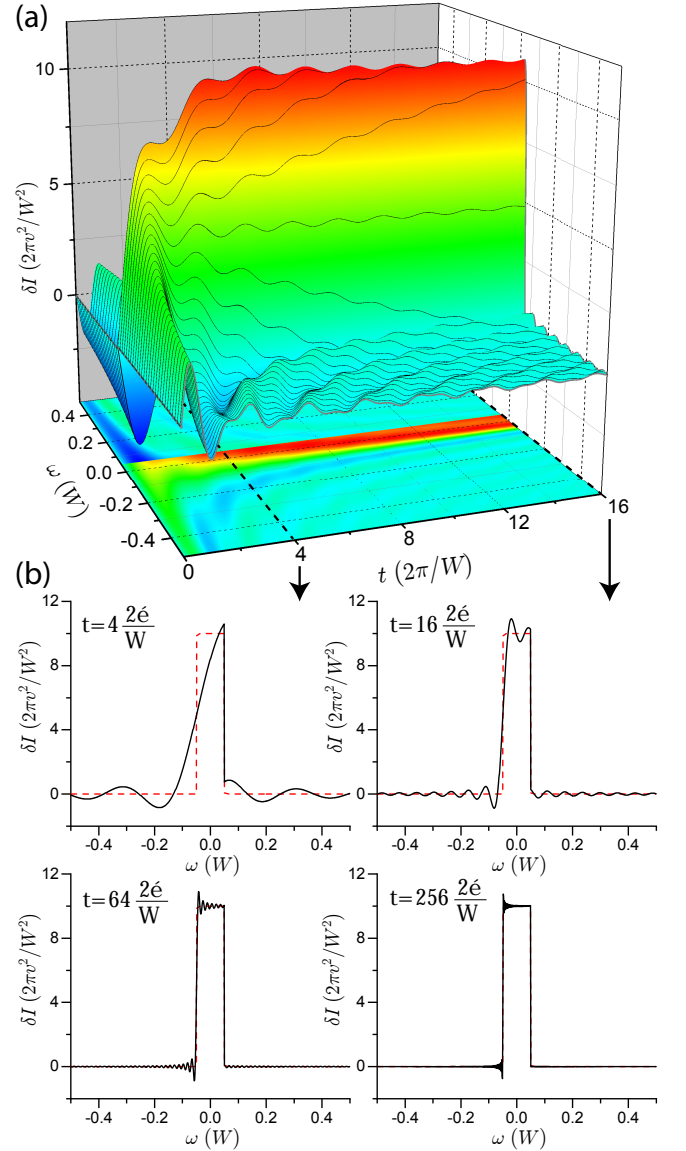

Figure 3. Current contribution, δI, from different frequencies in $\mathcal{L}$. (a) Initially, all states contribute substantially to the current, but contributions above and below the Fermi level partially cancel, see $I_\mathcal{L}$ and $I_\mathcal{R}$ in the Fig. 2 inset. (b) Contributions to the current for times t indicated on each panel. As $t \to \infty$, the contributions approach the red dashed line, with vanishing values outside the bias window, $-\mu/2 \leq \omega \leq \mu/2$. The oscillatory features on the left side of the bias window reflect the occurrence of Gibbs phenomenon. These oscillations do not disappear but rather get squeezed toward the jump at the bias window edge. No oscillations exist on the positive side due to the nature of that edge (a cutoff from the Fermi-Dirac occupation).

appears with a prefactor that is also the small frequency scale. Hence, while it takes time to rise, it has a small contribution to the total current. As a separate note, the convergence to the infinite system limit is non-monotonic purely due to the discrete nature of the states and filling[73], which gives insight into behavior observed in density functional theory calculations[74].

We can also examine the contribution to the current from

different frequency scales on the left, Eq. (11). All frequency scales contribute to the current for short times, see Fig. 3a, but this contribution decays with both frequency and time. By $t = 4 \cdot 2\pi/W$, the contribution is small outside the bias window and, as time progresses, it takes on the form of the bias window, Fig. 3b (the contributions reflect the band structure/couplings and thus are flat for the flat band model). When solving problems numerically, one reduces continuum reservoirs/environments into a finite, discrete number of components. The decay of the contribution with frequency (outside the bias window) suggests routes to alternative coarse grainings in frequency to enhance the simulation efficiency, as done in Ref. 75. The influence of different frequency scales will ultimately depend on details of the model (e.g., the presence of interactions, etc.), but we expect that the Kubo approach will help reveal the errors incurred by various coarse grainings. We leave this for future studies and instead focus on errors in estimating the steady-state value of the current.

The rise time of the current is rapid, indicating that already for small system sizes and times one can get a reasonably accurate value of the steady-state current (in the model here, taking the first maximum as an estimate of the steady-state current would only give a relative error of G, about 18 %). The slowly (algebraically) decaying nature of oscillations, though, influence the accuracy of further simulation. From Eq. (12), the asymptotic decay of the current to its steady state is[76]

$$-\frac{1}{t^2}\frac{2v^2}{W^2}\frac{8W\cos\left[\frac{Wt}{2}\right]\sin\left[\frac{\mu t}{2}\right] - 8\mu\cos\left[\frac{\mu t}{2}\right]\sin\left[\frac{Wt}{2}\right]}{W^2 - \mu^2},$$

(14)

compared with

$$-\frac{1}{t}\frac{2v^2}{N_\mathcal{L}W}\frac{W\cos[\omega_k t]\cos\left[\frac{Wt}{2}\right] + 2\omega_k\sin[\omega_k t]\sin\left[\frac{Wt}{2}\right]}{(W/2)^2 - \omega_k^2}$$

(15)

from Eq. (9) for a single particle going into an empty band. Both expressions are in the long-limit compared to all other timescales (namely, $1/\mu$ and $1/\omega_k$, as well as $1/W$). In the case of an infinitesimal bias ($1/\mu \to \infty$ before the long time limit), one also gets oscillations that decay as $1/t$ (specifically, $-4u\cos(Wt/2)/Wt$, as with the single particle at $\omega_k = 0$).

To obtain the steady state current, one has to deal with finite size and finite time issues, including both real physical effects (such as the decaying oscillations here) and artifacts (such as persistent oscillations due to finite lattice sizes[46]). One can remove persistent oscillations seen in impurity problems by fitting[46], reducing one source of uncertainty but there are still other finite-size errors. In the case here, fitting the decaying envelope of the oscillations to $1/T$ will give an accurate estimate of the steady state current. However, complex models will have much more complicated dynamics with oscillations at many time scales and amplitudes, and potentially with a different decay in time. Fitting, finding a bisecting line, or enveloping oscillations will be difficult to implement when the oscillations and decay are more irregular (although, a universal $1/T$ behavior appears in higher cumulants[77,78]). We thus assess "model agnostic" strategies – strategies that do not require specific knowledge of the model under study – to obtain
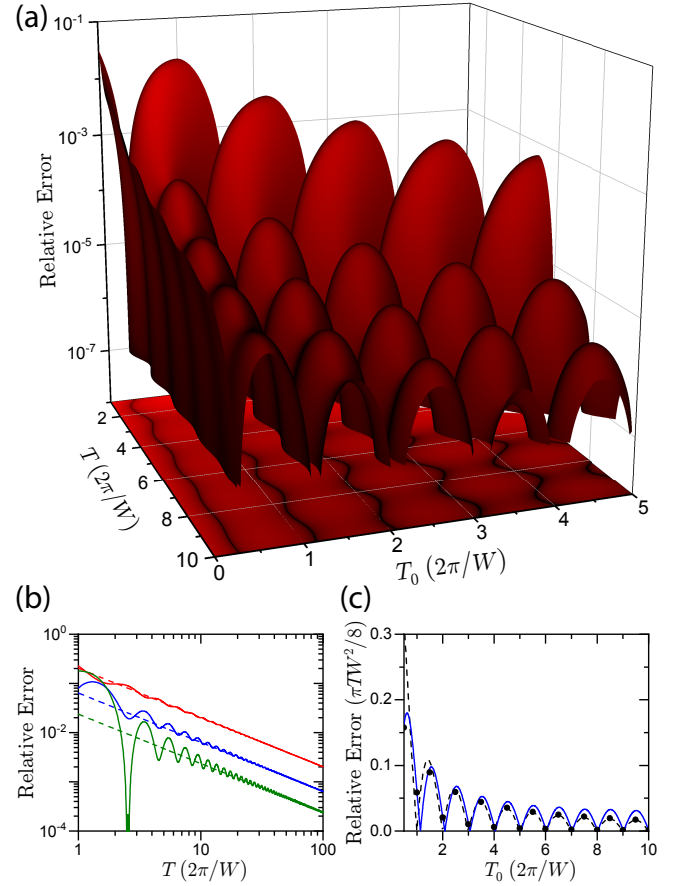

Figure 4. Relative error of the estimate, Eq. (17). (a) Error versus T and T_0. For a given total simulation time, T, the error has minima when T_0 is approximately integer multiples of $2\pi/W$. For long times (both T and T_0), the oscillations that can be seen on the 2D projection smooth to flat lines and the minima approach these values. (b) Error versus T for $T_0 = 0$, π/W, and $2\pi/W$ (solid red, blue, and green lines, respectively). All of these decay as $1/T$ for large T, shown by the asymptotic forms (dashed lines with the same colors). If T_0 is set to $3\pi/W$ (in between extrema), the error will be substantially larger than when it is $2\pi/W$ (at an extremum). (c) Error normalized by $1/T$. The blue line (black circles) shows $T = 20 \cdot 2\pi/W$ ($200 \cdot 2\pi/W$). The dashed, black line shows the asymptotic result, Eq. (18). So long as both T and T_0 are large enough, the asymptotic result captures the relative error. The minima in this limit are exactly at integer multiples of $2\pi/W$ for T_0 regardless of T (including non-integer multiples of $2\pi/W$).

the value of the steady state current that remove finite time effects, the ones shown to be limiting in related contexts[77].

Two agnostic strategies for estimating the steady state current from a closed, finite-sized simulation are to (1) take the value of the current at the end of the simulation or (2) average the current over some region of time. These approaches sometimes serendipitously yield the exact current. Thus, we will either work with error envelopes, i.e., the smooth curve going through the set of maxima in the error versus time, or with asymptotic forms for the error decay. Considering the relative error, $1 - I_{\text{sim}}/I_{\text{exact}}$ with I_{sim} the current from sim-

ulation and I_{exact} the exact current, strategy (1) gives

$$\frac{8}{\pi \mu W T^2} \qquad (16)$$

for the *error envelope*. Here, T is the total simulation time and we took $T \to \infty$ and then $\mu \to 0$ (taking the limit $\mu \to 0$ and then $T \to \infty$ gives a leading $1/T$ decay in the oscillations and error[79]). For strategy (2), the estimate is

$$I_{\text{sim}} = \frac{1}{T - T_0} \int_{T_0}^{T} I(t) \, dt. \qquad (17)$$

Compact forms for the relative error follow from integrating this equation with $I(t)$ from Eq. (10). To simplify calculations, we can work with the small bias expression directly in the case of strategy (2), as the average in Eq. (17) will have a dominant error due to short time contributions. The error will thus decay as $1/T$ so long as T_0 is not too large (i.e., either $T \to \infty$ and then $\mu \to 0$, or the reverse, will do).

Figure 4a shows the relative error versus T and T_0 for strategy (2). The minimum error comes at approximately integer multiples of $2\pi/W$ for T_0 – at oscillatory extrema of the current – for *any* value of T. Indeed, the asymptotic error decay (first $T \to \infty$ and then $T_0 \to \infty$),

$$\left| \frac{8 \sin(T_0 W/2)}{\pi W^2 T T_0} \right|, \qquad (18)$$

has minimal error exactly when T_0 is an integer multiple of $2\pi/W$. The reason for this is that the integration in Eq. (17) accumulates excess error (e.g., $I(t) > I_{\text{exact}}$) before encountering terms (e.g., $I(t) < I_{\text{exact}}$) that cancel that excess. The maximal cancellation of errors occurs when T_0 is at multiples of $2\pi/W$. If $T - T_0$ is a multiple of $4\pi/W$ (i.e., a complete oscillation), then there are saddle points on the error manifold when T_0 is at odd multiples of π/W, but moving T_0 toward the extrema (holding T constant) decreases further the error. Figures 4(b,c) show the error decay for different T_0 and the coefficient of the decay versus T_0. The asymptotic coefficient qualitatively captures even the non-asymptotic regime. For small T_0, though, the coefficient can be off in relative terms, which is not apparent on the scale of Fig. 4(c): Comparing Eq. (18) with $T_0 = 2\pi/W$ to the actual decay, $2(2 - \pi^2 G)/\pi W T$, for large T but not large T_0, it is clear that the actual coefficient of the decay is due to early time behavior (and hence why Gibbs' constant appears). It is the initial error that slowly decays away as T increases in the integration that plays the important role.

Given that strategy (2) has error decaying as $1/T$ and (1) as $1/T^2$, the latter is better for long simulations. However, in practice, large systems and times are inaccessible, i.e., simulations are typically in the range of 10 to 100 natural time units[23,28]. Thus, the coefficient of the decay matters. Since strategy (1) has higher error for small T, there is a crossing time when strategy (1) becomes better than (2). This crossing time is much greater than $100 \cdot 2\pi/W$ except for $T_0 = 0$, for which it comes at about $60 \cdot 2\pi/W$. Thus, averaging within a window (with T_0 at an extrema) is generally a better strategy. While these results are for the specific model under study, many-body systems can display the same decaying oscillations[23,?], including quantitatively in a large regime of many-body interaction induced transport[23] (which shows the Gibbs phenomenon and rapid develop of the steady state). Indeed, we closely followed (2) for many-body transport simulated with matrix product states[?], albeit empirically determined.

We emphasize that strategy matters, as even if the goal is only moderate accuracy (e.g., 1 %), different strategies can mean orders of magnitude longer simulations requiring an order of magnitude larger system, as the maximum simulation time[80] is proportional to N. If the computational cost scales as $T N^p$, where $p \geq 1$, then a 10 times longer simulation will mean at least a 100 times the computational cost[81].

The Kubo approach here elucidates the physics behind the development of the steady state and transient oscillations. These oscillations are none other than the Gibbs phenomenon due to the filtering of the current through the electronic bandwidth and bias window. Unlike the original context of the Gibbs phenomenon[67–71] (and in filtering signals), the ringing oscillations are not artifacts, but physical. For individual particles, the quasi-steady state is a manifestation of the wave-like nature of particles. However, for many particles, the current will near its steady state value in time π/W. This is why tensor network simulations of the current obtain reasonable results even for quite small simulations. We expect that the Kubo approach will assist in understanding other features of simulations, providing general guidance and informing new strategies for enhancing efficiency.

REFERENCES

[1] N. J. Tao, Nat. Nano. **1**, 173 (2006).

[2] H. Song, M. A. Reed, and T. Lee, Adv. Mater. **23**, 1583 (2011).

[3] E. Lörtscher, Nat. Nano. **8**, 381 (2013).

[4] M. Ratner, Nat. Nano. **8**, 378 (2013).

[5] L. Sun, Y. A. Diaz-Fernandez, T. A. Gschneidtner, F. Westerlund, S. Lara-Avila, and K. Moth-Poulsen, Chem. Soc. Rev. **43**, 7378 (2014).

[6] K. Wang and B. Xu, Top. Curr. Chem. **375**, 17 (2017).

[7] G. Platero and R. Aguado, Phys. Rep. **395**, 1 (2004).

[8] S. Kohler, J. Lehmann, and P. Hänggi, Phys. Rep. **406**, 379 (2005).

[9] G. Fève, A. Mahé, J. M. Berroir, T. Kontos, B. Plaçais, D. C. Glattli, A. Cavanna, B. Etienne, and Y. Jin, Science **316**, 1169 (2007).

[10] Z. Zhong, N. M. Gabor, J. E. Sharping, A. L. Gaeta, and P. L. McEuen, Nat. Nano. **3**, 201 (2008).

[11] D. R. Ward, N. J. Halas, J. W. Ciszek, J. M. Tour, Y. Wu, P. Nordlander, and D. Natelson, Nano Lett. **8**, 919 (2008).

[12] Y. Terada, S. Yoshida, O. Takeuchi, and H. Shigekawa, Nat. Photon. **4**, 869 (2010).

[13] B. Marquardt, M. Geller, B. Baxevanis, D. Pfannkuche, A. D. Wieck, D. Reuter, and A. Lorke, Nat. Commun. **2**, 209 (2011).

[14] A. M. Moore, S. Yeganeh, Y. Yao, S. A. Claridge, J. M. Tour, M. A. Ratner, and P. S. Weiss, ACS Nano **4**, 7630 (2010).

[15] S. Müllegger, S. Tebi, A. K. Das, W. Schöfberger, F. Faschinger, and R. Koch, Phys. Rev. Lett. **113**, 133001 (2014).

[16] J. Trasobares, D. Vuillaume, D. Théron, and N. Clément, Nat. Commun. **7**, 12850 (2016).

[17] T. L. Cocker, D. Peller, P. Yu, J. Repp, and R. Huber, Nature **539**, 263 (2016).

[18] S. Giorgini, L. P. Pitaevskii, and S. Stringari, Rev. Mod. Phys. **80**, 1215 (2008).

[19] I. Bloch, J. Dalibard, and W. Zwerger, Rev. Mod. Phys. **80**, 885 (2008).

[20] U. Schneider, L. Hackermuller, J. P. Ronzheimer, S. Will, S. Braun, T. Best, I. Bloch, E. Demler, S. Mandt, D. Rasch, and A. Rosch, Nat. Phys. **8**, 213 (2012).

[21] C.-C. Chien, M. Zwolak, and M. Di Ventra, Phys. Rev. A **85**, 041601 (2012).

[22] J.-P. Brantut, J. Meineke, D. Stadler, S. Krinner, and T. Esslinger, Science **337**, 1069 (2012).

[23] C.-C. Chien, D. Gruss, M. Di Ventra, and M. Zwolak, New J. Phys. **15**, 063026 (2013).

[24] C.-C. Chien, M. Di Ventra, and M. Zwolak, Phys. Rev. A **90**, 023624 (2014).

[25] S. Krinner, D. Stadler, D. Husmann, J.-P. Brantut, and T. Esslinger, Nature **517**, 64 (2015).

[26] C.-C. Chien, S. Peotta, and M. Di Ventra, Nat. Phys. **11**, 998 (2015).

[27] S. Krinner, T. Esslinger, and J.-P. Brantut, J. Phys.: Condens. Matter **29**, 343003 (2017).

[28] D. Gruss, C.-C. Chien, J. T. Barreiro, M. D. Ventra, and M. Zwolak, New J. Phys. **20**, 115005 (2018).

[29] A. Eckardt, Rev. Mod. Phys. **89**, 011004 (2017).

[30] P. Weinberg, M. Bukov, L. D'Alessio, A. Polkovnikov, S. Vajna, and M. Kolodrubetz, Phys. Rep. **688**, 1 (2017).

[31] M. Zwolak and G. Vidal, Phys. Rev. Lett. **93**, 207205 (2004).

[32] M. Di Ventra and T. N. Todorov, J. Phys.: Condens. Matter **16**, 8025 (2005).

[33] N. Bushong, N. Sai, and M. Di Ventra, Nano Lett. **5**, 2569 (2005).

[34] G. Schneider and P. Schmitteckert, arXiv:cond-mat/0601389 (2006).

[35] P. Schmitteckert and G. Schneider, in *High Performance Computing in Science and Engineering*, edited by W. E. Nagel, W. Jäger, and M. Resch (Springer, Berlin, 2006) pp. 113–126.

[36] C.-L. Cheng, J. S. Evans, and T. Van Voorhis, Phys. Rev. B **74**, 155112 (2006).

[37] K. A. Al-Hassanieh, A. E. Feiguin, J. A. Riera, C. A. Büsser, and E. Dagotto, Phys. Rev. B **73**, 195304 (2006).

[38] N. Bushong, J. Gamble, and M. Di Ventra, Nano Lett. **7**, 1789 (2007).

[39] N. Sai, N. Bushong, R. Hatcher, and M. Di Ventra, Phys. Rev. B **75**, 115410 (2007).

[40] L. G. G. V. Dias da Silva, F. Heidrich-Meisner, A. E. Feiguin, C. A. Büsser, G. B. Martins, E. V. Anda, and E. Dagotto, Phys. Rev. B **78**, 195317 (2008).

[41] J. S. Evans, O. A. Vydrov, and T. Van Voorhis, J. Chem. Phys. **131**, 034106 (2009).

[42] H. Eshuis and T. van Voorhis, Phys. Chem. Chem. Phys. **11**, 10293 (2009).

[43] F. Heidrich-Meisner, A. E. Feiguin, and E. Dagotto, Phys. Rev. B **79**, 235336 (2009).

[44] P. Myöhänen, A. Stan, G. Stefanucci, and R. van Leeuwen, Phys. Rev. B **80**, 115107 (2009).

[45] S. Kurth, G. Stefanucci, E. Khosravi, C. Verdozzi, and E. K. U. Gross, Phys. Rev. Lett. **104**, 236801 (2010).

[46] A. Branschädel, G. Schneider, and P. Schmitteckert, Ann. Phys. (Berlin) **522**, 657 (2010).

[47] Y. Wang, C. Y. Yam, T. Frauenheim, G. H. Chen, and T. A. Niehaus, Chem. Phys. **391**, 69 (2011).

[48] K. Varga, Phys. Rev. B **83**, 195130 (2011).

[49] B. Gaury, J. Weston, M. Santin, M. Houzet, C. Groth, and X. Waintal, Phys. Rep. **534**, 1 (2014).

[50] D. Gruss, K. A. Velizhanin, and M. Zwolak, Sci. Rep. **6**, 24514 (2016).

[51] D. Gruss, A. Smolyanitsky, and M. Zwolak, J. Chem. Phys. **147**, 141102 (2017).

[52] J. E. Elenewski, D. Gruss, and M. Zwolak, J. Chem. Phys. **147**, 151101 (2017).

[53] K. A. Velizhanin, S. Sahu, C.-C. Chien, Y. Dubi, and M. Zwolak, Sci. Rep. **5**, 17506 (2015).

[54] C.-C. Chien, S. Kouachi, K. A. Velizhanin, Y. Dubi, and M. Zwolak, Phys. Rev. E **95**, 012137 (2017).

[55] C.-C. Chien, K. A. Velizhanin, Y. Dubi, B. R. Ilic, and M. Zwolak, Phys.

[56] Rev. B **97**, 125425 (2018).

[56] C. G. Sánchez, M. Stamenova, S. Sanvito, D. R. Bowler, A. P. Horsfield, and T. N. Todorov, J. Chem. Phys. **124**, 214708 (2006).

[57] J. E. Subotnik, T. Hansen, M. A. Ratner, and A. Nitzan, J. Chem. Phys. **130**, 144105 (2009).

[58] T. Zelovich, L. Kronik, and O. Hod, J. Chem. Theory Comput. **10**, 2927 (2014).

[59] T. Zelovich, T. Hansen, Z.-F. Liu, J. B. Neaton, L. Kronik, and O. Hod, J. Chem. Phys. **146**, 092331 (2017).

[60] U. N. Morzan, F. F. Ramirez, M. C. G. Lebrero, and D. A. Scherlis, J. Chem. Phys. **146**, 044110 (2017).

[61] For instance, the approach captures negative differential conductance when a bias is switched on simultaneously with the weak link. There is, of course, a change in the chemical potential with time due to having finite systems, which is not captured by the approach.

[62] D. Bohr, P. Schmitteckert, and P. Wölfle, Europhys. Lett. **73**, 246 (2006).

[63] D. Bohr and P. Schmitteckert, Phys. Rev. B **75**, 241103 (2007).

[64] P. Schmitteckert and F. Evers, Phys. Rev. Lett. **100**, 086401 (2008).

[65] If the coupling from state k to $\mathcal{R}$ was given by the spectral function $\gamma/2\pi$ (i.e., flat but unbounded when $W \to \infty$), then $n_k(t)$ will be exponentially decaying even for short times[75].

[66] A.-P. Jauho, N. S. Wingreen, and Y. Meir, Phys. Rev. B **50**, 5528 (1994).

[67] H. Wilbraham, Cambridge and Dublin Math. J. **3**, 198 (1848).

[68] J. W. Gibbs, Nature **59**, 200 (1898).

[69] J. W. Gibbs, Nature **59**, 606 (1899).

[70] M. Bocher, Ann. Math. **7**, 81 (1906).

[71] E. Hewitt and R. E. Hewitt, Arch. Hist. Exact Sci. **21**, 129 (1979).

[72] The contribution from the cosine component of the inverse Fourier transform is zero. However, working directly with Eq. (6), i.e., without first taking the imaginary component, the integral of $(\cos[t(\omega_k - \omega')] - 1)/(\omega_k - \omega')$ yields a non-zero real component. This is not part of the signal of interest. We note that the v^2 contribution to the prefactor can be written as $v^2\Theta(t)$, which properly removes the signal for $t < 0$.

[73] The total coupling of modes in the bias window determines the current magnitude. Each mode can be thought of taking up $\Delta = W/N$ width of the spectral density. For even N and placing the modes uniformly across the total bandwidth $(-W/2 + \Delta/2 + (k-1)\Delta$, with $k = 1, \ldots, N)$, the number of modes in the bias window is $n = 2 \cdot \text{Floor}[N\mu/2W + 1/2]$ when the bias is applied symmetrically ($\mu_{\mathcal{L}} = -\mu_{\mathcal{R}} = \mu/2$). To obtain the proper steady state current, the fraction of the spectral density in the bias window must be equal to the bias as a fraction of the bandwidth, $n/N \equiv \mu/W$. After rearranging, $N\mu/2W = n/2$ or, in other words, $N\mu/2W$ has to be an integer (n is even). When $N\mu/2W$ is not an integer, the modes in the bias window have $n/N \lessgtr \mu/W$ and therefore either they underestimate or overestimate the current. Note, as well, that $N\mu/2W = \text{Integer}$ is a purely artificial constraint to get the right coupling strength (and hence current) for finite-size systems. As $N \to \infty$, the corrections away from integer values decay as $1/N$. While these results are for the flat band model with equally spaced modes, the calculation can be done in other scenarios as well (more complex band structures and couplings, and potentially even out of the weak coupling limit by checking finite-size convergence of the Greens functions). .

[74] Z. Yang, A. Tackett, and M. Di Ventra, Phys. Rev. B **66**, 041405 (2002).

[75] M. Zwolak, J. Chem. Phys. **129**, 101101 (2008).

[76] Equation (12) has an explicit oscillatory term that decays as $1/t$. However, this cancels the highest order (in $1/t$) term from the sine integrals.

[77] P. Schmitteckert, S. T. Carr, and H. Saleur, Phys. Rev. B **89**, 081401 (2014).

[78] S. T. Carr, P. Schmitteckert, and H. Saleur, Phys. Scr. **2015**, 014009 (2015).

[79] The appropriate limit depends on the bias and time range of interest. For $\mu = W/10$ and times past $10 \cdot 2\pi/W$, $T \to \infty$ should be first.

[80] Equation (7) has contributions that recur at a time $\pi N/W$ – in this case taken as the time, $t \cdot W/N = \pi$, that a positive contribution turns negative, where W/N is the level spacing. In natural time units ($2\pi/W$), this time is $N/2$.

[81] For correlation matrices, $p = 2$ or 3 depending on locality of hopping. For numerical renormalization, formally $p = 1$, but longer simulations generate additional entanglement that gives an effective p that is larger.